Line Topology Identification Using Multiobjective Evolutionary Computation

Claudomiro Sales, Roberto M. Rodrigues, Fredrik Lindqvist, João Costa, *Member, IEEE*, Aldebaro Klautau, *Senior Member, IEEE*, Klas Ericson, Jaume Rius i Riu, and Per Ola Börjesson

***Abstract*—The broadband capacity of the twisted-pair lines strongly varies within the copper access network. It is therefore important to assess the ability of a digital subscriber line (DSL) to support the DSL services prior to deployment. This task is handled by the line qualification procedures, where the identification of the *line topology* is an important part. This paper presents a new method, denoted topology identification via model-based evolutionary computation (TIMEC), for line topology identification, where either one-port measurements or both one- and two-port measurements are utilized. The measurements are input to a model-based multiobjective criterion that is minimized by a genetic algorithm to provide an estimate of the line topology. The inherent flexibility of TIMEC enables the incorporation of a priori information, e.g., the total line length. The performance of TIMEC is evaluated by computer simulations with varying degrees of information. Comparison with a state-of-art method indicates that TIMEC achieves better results for all the tested lines when only one-port measurements are used. The results are improved when employing both one- and two-port measurements. If a rough estimate of the total length is also used, near-perfect estimation is obtained for all the tested lines.**

***Index Terms*—Digital subscriber line (DSL), double-ended line testing (DELT), evolutionary computation, line qualification (LQ), line topology identification, multiobjective optimization, single-ended line testing (SELT).**

I. Introduction

THROUGH the years, several types of digital subscriber line (DSL) technologies have been standardized for broadband data transmission on the twisted-pair lines (loops), e.g., asymmetric DSL (ADSL) and very-high-bit-rate DSL.

Manuscript received January 12, 2009; revised April 12, 2009. First published September 22, 2009; current version published February 10, 2010. This work was supported in part by the Swedish Agency for Innovation Systems (VINNOVA) through the Eureka–Celtic BANITS Project and in part by the Research and Development Centre, Ericsson Telecomunicações S.A., Brazil. The Associate Editor coordinating the review process for this paper was Dr. John Sheppard.

C. Sales and R. M. Rodrigues are with the Institute of Technology, Federal University of Para, 66075-110 Belem, Brazil (e-mail: cssj@ufpa.br; menegues@ufpa.br).

F. Lindqvist is with the Department of Electrical and Information Technology, Lund University, 221 00 Lund, Sweden and also with Ericsson A.B., 164 80 Stockholm, Sweden (e-mail: fredrik.lindqvist@eit.lth.se).

J. Costa and A. Klautau are with the Electrical Engineering Graduate Program, Institute of Technology, Federal University of Para, 66075-110 Belem, Brazil (e-mail: jweyl@ufpa.br; aldebaro@ufpa.br).

K. Ericson and J. R. i Riu are with the Broadband Technologies Laboratory/Department, Ericsson AB, 23 16480 Stockholm, Sweden (e-mail: klas.ericson@ericsson.com; jaume.rius.i.riu@ericsson.com).

P. O. Börjesson is with the Department of Electrical and Information Technology, Lund University, 221 00 Lund, Sweden (e-mail: per.ola.borjesson@eit.lth.se).

Digital Object Identifier 10.1109/TIM.2009.2025991

The broadband capacity of the lines strongly varies within the copper access network, because it was originally designed for narrowband analog transmission, i.e., plain old telephony service (POTS). Features such as bridged taps, load coils, and mixed cable types [1] have been introduced in the network to improve or extend the POTS. For DSL transmission, however, which exploits a much wider frequency range, these features affect the service quality. It is therefore important to assess the ability of a line to support the DSL services prior to deployment. This task is handled by the line qualification (LQ) procedures.

The existing POTS equipments are normally limited to the bandwidth from direct current up to 4 kHz. This fact makes them less suitable to accurately qualify a line for broadband transmission. New broadband techniques that target LQ for DSL have therefore been proposed, for example, in [2]–[5].

The legacy POTS methods for LQ are typically restricted to estimating the total line length. Service activation is then based on predefined deployment rules, which define the maximum line lengths for proper deployment of a specific DSL service [6]. Alternatively, the topology of the line under test can be identified, which corresponds to the determination of the number of sections, wire diameter (gauge), and length of each section. The line topology identification also includes identifying the number of bridged taps (if they exist), as well as their positions and lengths. Although this task is challenging, an accurate estimate of the line topology enables efficient LQ, where any existing line databases can be corrected and updated. The databases can thereafter be used for support-engineering, provisioning, and maintenance operations [4].

Line topology identification methods may employ two kinds of testing approaches: 1) single-ended line testing (SELT), where one-port measurements are performed, for example, from the central office (CO) side of the line, and 2) double-ended line testing (DELT), which is based on two-port measurements that require communication between the CO and the customer premises (CPs) equipment.

Most line topology identification methods in the literature are focused on SELT with time-domain reflectometry (TDR) or frequency-domain reflectometry. Both techniques are based on transmitting a probe signal, followed by a posterior analysis of the occurring reflection trace [4], [7]. In [2], a model for analyzing the real and spurious echoes is proposed, as well as a way of extracting the intrinsic slowly decaying signal from the reflectogram. This approach enables an improved detection of weak echoes. In [4], an iterative de-embedding process for the TDR reflectogram is proposed, where the type

of discontinuities is first identified using a database and the mean-square-error criterion, followed by an estimate of the section lengths. In [8], the method in [4] is evaluated using measurements that were obtained by differential TDR. The line topology identification approach in [9] is based on the measured one-port scattering parameter $S_{11}(f)$. This approach utilizes preprocessing to obtain an appropriate time-domain response $s_{11}(t)$ [5], from which important features are extracted, e.g., time delay, amplitude, and energy, [9], [10]. The extracted features are further used by an automated interpreting system based on Bayesian networks to estimate the line topology.

In [3], a DELT method for bridged-tap location using transfer function measurements is described. Previously, this method would have been impractical for mass deployment due to the high cost of dedicated equipment necessary at the customer site. However, with the recent advent of the Telecommunication Standardization Sector (ITU-T) standards for ADSL2 and ADSL2+, [11], [12], DELT has become a mandatory facility, which was denoted as loop diagnostic in [11] and [12]. Thus, standard compliant modems, which were located at the customer side, can communicate with the modem at the CO side to perform DELT. Measurements such as two-port channel transfer function $H(f)$ are possible through DELT, where the lower frequency part is measured from the CP to the CO, and the upper part is measured from the CO to the CP.

Some of the previously published line topology identification methods rely on a priori information to achieve accurate results [3]–[5]. This information can consist of, e.g., a database of installed cables or the frequency-dependent velocity of propagation. It is intuitive that a priori information can be helpful, but in many practical applications, such information is not available or not reliable. Hence, it is desirable to design methods that are not dependent on a priori information but, at the same time, are flexible to accommodate such information when available.

This paper describes a methodology for line topology identification, which employs SELT and, if supported, DELT. The proposed method utilizes the obtained one- and two-port measurements to compose a model-based multiobjective criterion. The criterion is minimized by a specialized version of the nondominated sorting genetic algorithm (NSGA-II) [13] that seeks the topology that best matches the defined criterion. The inherent flexibility of the proposed method allows the integration of available a priori information. The proposed method is evaluated by computer simulations based on either one-port measurements or both one- and two-port measurements. The performance of the proposed method is evaluated by computer simulations with varying degrees of information. By using simulated measurements, a controlled environment is established, which is suitable for the analysis of results.

The remainder of this paper is organized as follows. Section II provides a description of the proposed line topology identification method. Section III presents the specializations on the conventional genetic algorithm (GA) to improve the rate of convergence and the accuracy. Section IV presents the simulation results for the test lines. Finally, the summary and conclusions are given in Section V.

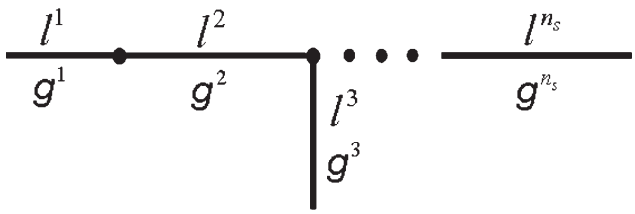

Fig. 1. Set of parameters Θ of a given line that will be determined. In this example, the third section of the illustrative line is a bridged tap, whereas the first, second, and last ones are *serial*.

II. Proposed Method

The proposed method estimates the line topology based on two frequency-dependent quantities: 1) the SELT-measured scattering parameter $\hat{S}_{11}$ and 2) the DELT-measured transfer function $\hat{H}$. The frequency dependence of these quantities is omitted in the notation for simplicity. Alternatively, the SELT-measured input impedance of the line could be used in place of $\hat{S}_{11}$, but paper work will assume $\hat{S}_{11}$. In case only SELT measurements are available, the transfer function and associated formulas, which were described as follows, are not used. In particular, the task is to estimate the set of parameters Θ that characterize (model) a given line. In this paper, Θ is defined as the set that contains the following components, as illustrated in Fig. 1:

1) number of line sections n_s;
2) length of each section l;
3) gauge (diameter) of each section g;
4) type of each section (Boolean) b, i.e., serial or bridged tap.

In particular, Θ is a set of subsets, i.e., $\Theta = \{\theta^{(1)}, \theta^{(2)}, \ldots, \theta^{(n_s)}\}$, where the subset $\theta^{(k)} = \{l^k, g^k, b^k\}$ contains the length, gauge, and type of the kth section.

For estimation, an *analysis-by-synthesis* process is adopted in this paper. That is, for a given candidate solution Θ and an assumed cable model, the classic two-port network theory (for example, see [1]) is used to derive the corresponding modeled S_{11} and H. These two quantities are then compared to the measured $\hat{S}_{11}$ and $\hat{H}$ by using the objective (cost) functions $V_H(\Theta)$ and $V_{S_{11}}(\Theta)$. The true parameters will be denoted by $\Theta^\dagger$, whereas a candidate solution is denoted by Θ. A GA-based optimization routine then iteratively seeks the best solution Θ^* based on the two objective functions. The goal is to obtain $\Theta^* = \Theta^\dagger$, but imperfections on measurements and/or modeling can obviously impact the results. This paper considers only errors that were due to topology mismatch, because measurements are replaced with noiseless computer simulations. The reader is referred to Appendix A for a more detailed error analysis.

The next three sections provide a brief review of the two-port network theory and a description of the proposed method, called *topology identification via model-based evolutionary computation* (TIMEC). Evolutionary computation is the collective name for algorithms that were inspired by biological evolution. This paper discusses only GAs [14]–[16], but the proposed approach can be used with the optimization that was performed by other evolutionary algorithms.

A. Classic Two-Port Network Theory

Each line section, which is represented by the $\theta^{(k)}$ of a candidate solution Θ, is considered a homogeneous transmission line and can therefore be modeled as a two-port network, which is represented by its frequency-dependent transmission $ABCD$ matrix. In particular, a serial section is modeled by [1], [17]

$$\mathbf{T}_s = \begin{bmatrix} A & B \\ C & D \end{bmatrix} = \begin{bmatrix} \cosh(\gamma l) & Z_0 \sinh(\gamma l) \\ \frac{\sinh(\gamma l)}{Z_0} & \cosh(\gamma l) \end{bmatrix} \tag{1}$$

whereas a bridged tap is modeled by

$$\mathbf{T}_{bt} = \begin{bmatrix} A & B \\ C & D \end{bmatrix} = \begin{bmatrix} 1 & 0 \\ \frac{\tanh(\gamma l)}{Z_0} & 1 \end{bmatrix} \tag{2}$$

where l is the corresponding section length, γ is the propagation constant, and Z_0 is the characteristic impedance. Note that γ and Z_0 are frequency-dependent complex values, but for simplicity, this dependency is not indicated here for H and S_{11}. The nominal values for γ and Z_0 are obtained from an assumed cable model, e.g., University Vrije Universiteit Brussel (VUB) [18], MAR [19], British Telecom (BT) [19], or $\mathrm{BT0_H}$ [20]. These models have inherent electromagnetic and geometrical parameters that characterize the insulation material, resistivity, and other factors. In this paper, however, we will only use the VUB [18] model with γ and Z_0 completely defined by the wire gauge, as described in Appendix B. It is therefore only necessary to include the wire gauge as a parameter in Θ. In general, one may extend Θ to also include some of the inherent cable parameters. However, this extension is beyond the scope of this paper.

For a line with different sections, the chain rule [1] can be applied to obtain the overall transmission matrix. That is, for a line with n_s number of sections, the overall (forward) transmission matrix $\mathbf{T}_f$ is given by the following matrix product:

$$\mathbf{T}_f = \mathbf{T}^{(1)} \cdot \mathbf{T}^{(2)} \cdot \ \cdots \ \cdot \mathbf{T}^{(n_s)}. \tag{3}$$

Based on matrix $\mathbf{T}_f$, it is possible to derive the quantities of interest. In particular, the scattering parameter S_{11} and the transfer function H, which corresponds to Θ, can be formulated as [17]

$$S_{11} = \frac{AZ_L + B - CZ_SZ_L - DZ_S}{AZ_L + B + CZ_SZ_L + DZ_S} \tag{4}$$

$$H = \frac{Z_L}{AZ_L + B + CZ_SZ_L + DZ_S} \tag{5}$$

where Z_S and Z_L are the source and load impedances, respectively, and A, B, C, and D are the frequency-dependent elements of the overall transmission matrix $\mathbf{T}_f$.

In summary, given a set of parameters Θ that describe a line, the two quantities H and S_{11} are generated using the aforementioned two-port network theory and a cable model. In this paper, this generation process is represented by the operator $\mathcal{V}$ as

$$[H, S_{11}] = \mathcal{V}\{\Theta\}. \tag{6}$$

B. GA-Based Optimization

Several optimization routines can be applied within the proposed analysis-by-synthesis framework. GA is chosen, because it is flexible and well suited for the optimization of multidimensional spaces with many local optima. GA does not require properties such as convexity. On the other hand, the successful application of GA to a new problem typically depends on properly adapting the formalism to the specificities of the problem. This section briefly describes a general application of GA to the line topology identification problem, whereas Section III describes the developed modifications to improve the accuracy and convergence of the proposed method.

The DSL transceivers in this paper employ discrete multitone modulation, where the measurement bandwidth is divided into K frequencies or tones [1] (e.g., $K = 512$ for ADSL2+). This approach enables measurement of the quantities $S_{11}(f_k)$ and $H(f_k)$ through SELT and DELT at the frequency f_k for $k = 1, 2, \ldots, K$.

In this paper, the quantities that were associated with a candidate line Θ are compared with the measured (*target*) quantities, as defined by the following objective functions [21]:

$$V_H(\Theta) = \sum_{k=1}^{K} \frac{\left| H(\Theta, f_k) - \hat{H}(f_k) \right|^2}{\sigma^2_{\hat{H}}(f_k)} \tag{7}$$

$$V_{S_{11}}(\Theta) = \sum_{k=1}^{K} \frac{\left| S_{11}(\Theta, f_k) - \hat{S}_{11}(f_k) \right|^2}{\sigma^2_{\hat{S}_{11}}(f_k)} \tag{8}$$

where $\sigma_{\hat{S}_{11}}(f_k)$ and $\sigma_{\hat{H}}(f_k)$ are the standard deviations that were associated with the measured scattering parameter and the transfer function, respectively. These two standard deviations are used to weigh the error along the frequency according to the accuracy of the measurement and are obtained by conducting several measurements of each quantity. In case only one measurement of each quantity is available, $\sigma_{\hat{S}_{11}}(f_k) = \sigma_{\hat{H}}(f_k) = 1, \forall\, f_k$, is assumed.

Two objective functions are used in this paper; thus, multiobjective optimization is performed. Frequently, in multiobjective optimization, the defined objective functions are conflicting in the sense that there exists an ambiguity in the (final) optimum solution. For example, in our case with two objective functions, it is obvious that a solution Θ_a is better than Θ_b if $V_H(\Theta_a) < V_H(\Theta_b)$ and $V_{S_{11}}(\Theta_a) < V_{S_{11}}(\Theta_b)$. However, situations such as $V_H(\Theta_a) > V_H(\Theta_b)$ and $V_{S_{11}}(\Theta_a) < V_{S_{11}}(\Theta_b)$ are common. Thus, instead of providing one final solution, the multiobjective optimization provides a set of (optimum) solutions, which reflects the interaction between the different objectives. To deal with this case, the multiobjective optimization algorithm NSGA-II [13] is adopted in this paper. NSGA-II is based on the Pareto front selection [13]. The sorting of solutions in Pareto fronts is a useful formalism for letting the optimum solutions evolve along the optimization process. Therefore, at the end of the optimization, a set Ψ that corresponds to the solutions in the first Pareto front is selected, and a decision rule is employed to choose the final solution.

In this paper, the following strategy is adopted. First, the best candidate solution that was associated with each objective

function is selected from all candidates Θ_r that belong to the first Pareto front, i.e.,

$$\Theta_H^* = \arg \min_{r=1,2,\ldots,|\Psi|} V_H(\Theta_r)$$
$$\Theta_{S_{11}}^* = \arg \min_{r=1,2,\ldots|\Psi|} V_{S_{11}}(\Theta_r).$$

Then, the final solution is chosen as the option with the smallest sum of the objective functions, i.e.,

$$\Theta^* = \arg \min_{\Theta=\Theta_H^*,\Theta_{S_{11}}^*} \left(V_H(\Theta) + V_{S_{11}}(\Theta)\right). \tag{9}$$

Alternative strategies that provide different weights to the two objective functions can also be used.

A brute-force search for Θ^*, which exhaustively tries each possible set Θ, is unfeasible because of the huge size of the search space. However, GA avoids this problem by keeping a set (*population* in GA terminology) Φ of candidates and iteratively improving them along the iterations (*generations* in GA terminology).

The next section provides a description that was oriented toward the implementation of the proposed method on a computer.

C. Implementation of TIMEC

A flowchart with a high-level description of TIMEC is shown in Fig. 2, in accordance with the definition of the parameters and variables in Tables I and II.

In the initialization, the GA *control parameters* are initialized to their maximum values, i.e., $p_m = P_m$, $p_c = P_c$, and $\sigma_m = \Sigma_m$. If there is no a priori information about the line under test, Γ is initialized to the empty set, i.e., $\Gamma = \{\cdot\}$. An initial population Φ is randomly generated with size $R = |\Phi|$, where $|\cdot|$ is the number of elements (cardinality) of the set. To deal with the set of parameters Θ, GA requires mapping it into a coded structure called *chromosome*, which is composed of *genes*. The coding function $\mathcal{G}$ maps the line parameters Θ into the coded chromosome $\mathcal{G}(\Theta)$, and $\mathcal{G}^{-1}$ denotes the decoding operation. The initial population Φ is a set of chromosomes, and the values of the objective functions that were related to them are calculated by applying the operator $\mathcal{V}$ in (6) to all decoded parameters $\mathcal{G}^{-1}(\Phi) = \{\Theta_1, \ldots, \Theta_R\}$ and then using (7) and (8). The values of the objective functions are organized in an objective matrix $\mathbf{Q}$ according to

$$\mathbf{Q} = \begin{bmatrix} V_H(\Theta_1) & V_{S_{11}}(\Theta_1) \\ V_H(\Theta_2) & V_{S_{11}}(\Theta_2) \\ \vdots & \vdots \\ V_H(\Theta_R) & V_{S_{11}}(\Theta_R) \end{bmatrix} \tag{10}$$

with dimension $R \times 2$. Once the initial population of chromosomes Φ and the matrix $\mathbf{Q}$ have been generated, the first generation $(n = 1)$ starts.

As shown in Fig. 2, NSGA-II iteratively improves Φ until the final solution Θ^* is found. In particular, in each generation n, the GA operators (selection, mutation, and crossover) are applied to Φ to generate another population Φ'. The control parameters p_m, p_c, and σ_m are adapted using a novel algorithm,

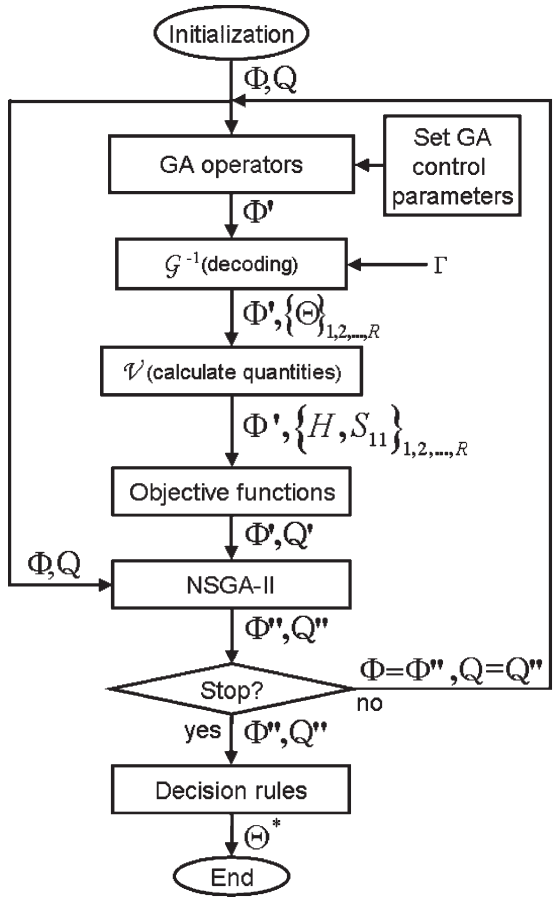

Fig. 2. Flowchart of the proposed method for line topology identification.

TABLE I
BRIEF DESCRIPTION OF THE EMPLOYED SYMBOLS: USER-DEFINED PARAMETERS

SYMBOL	DESCRIPTION
Σ_m	Maximum standard deviation of mutation
P_m	Maximum mutation probability
P_c	Maximum crossover probability
w	Weight that affects the time-changes of the GA control parameters
R	Size of the populations (Φ, Φ' and Φ'')
N	Maximum number of generations to be executed. This value can be modified during the optimization process
ΔN	Increment of the number of generations
δ	Threshold for the sum of the two objective functions
δ_{pc}	Decreasing rate factor for crossover probability
δ_{pm}	Decreasing rate factor for mutation probability
δ_{σ_m}	Decreasing rate factor for standard deviation of mutation
N_s	Maximum number of sections
$N_s^{\min}$	Minimum number of sections
$N_b^{\min}$	Minimum number of bridged-taps

TABLE II
BRIEF DESCRIPTION OF THE EMPLOYED SYMBOLS: DATA STRUCTURES AND VARIABLES

SYMBOL	DESCRIPTION
Γ	Store *a priori* information about the line under test
p_m	Current mutation probability
p_c	Current crossover probability
σ_m	Current standard deviation of mutation
Φ	Population (set) of chromosomes
Φ', Φ''	Temporary populations
$\mathbf{Q}$	Objective matrix. It stores the values of the objective functions related to the population Φ
$\mathbf{Q}'$, $\mathbf{Q}''$	Temporary objective matrices
n	Counter for the number of generations
$\tilde{\Theta}_H$	Candidate with current lowest value of the objective function related to the transfer function
$\tilde{\Theta}_{S_{11}}$	Candidate with current lowest value of the objective function related to the scattering parameter S_{11}
Θ^*	Final solution (identified topology of the line under test)
$\hat{H}$	Measured transfer function
H	Transfer function related to a certain candidate, calculated using the two-port network theory and a cable model
$\hat{S}_{11}$	Measured one-port scattering parameter S_{11}
S_{11}	One-port scattering parameter S_{11} related to a certain candidate, calculated using the two-port network theory and a cable model
Ω	Set containing the current values for the GA control parameters
Ψ	Solutions of the first Pareto front
n_s	Effective number of sections
n_b	Effective number of bridged-taps
c	Counter for the number of consecutive generations without evolution of the best chromosomes

as described in Section III-B. To calculate the quantities H and S_{11} with $\mathcal{V}$ in (6), each chromosome $\mathcal{G}(\Theta)$ must be decoded into the corresponding line parameters Θ. Proper coding/decoding is therefore crucial, and the proposed schemes are described in detail in Section III-A. If a priori information is available, i.e., $\Gamma \neq \{\cdot\}$, this information is used during the decoding process. The decoding block provides to the GA process both the new chromosomes Φ' and their decoded parameters $\mathcal{G}^{-1}(\Phi') = \{\Theta'_1, \ldots, \Theta'_R\}$. After decoding, the operator $\mathcal{V}$ in (6) is applied on the set $\{\Theta'_1, \ldots, \Theta'_R\}$ to calculate the corresponding quantities H and S_{11} associated with each chromosome in the set Φ'. The matrix $\mathbf{Q}'$ is obtained by comparing these quantities with the measured $\hat{H}$ and $\hat{S}_{11}$ through the respective objective function. Both the original and the new populations, i.e., Φ and Φ', and their respective objective matrices $\mathbf{Q}$ and $\mathbf{Q}'$ are used by the NSGA-II process to generate the resulting population Φ'' and its respective objective matrix $\mathbf{Q}''$.

In this paper, two stop conditions are employed. If the generation number n is larger than the maximum allowed number of generations N, i.e., $n > N$, the optimization is stopped. Moreover, if the sum of the objective functions associated with the best candidate solutions is less than a user-defined threshold δ, the optimization is also stopped. In essence, parameter δ controls the tradeoff between the rate of convergence and the accuracy of optimization. If none of the stop conditions is satisfied, i.e., $n \leq N$ and $V_H(\tilde{\Theta}_H) + V_{S_{11}}(\tilde{\Theta}_{S_{11}}) \geq \delta$, the new population Φ'' and the objective matrix $\mathbf{Q}''$ replace the current population Φ and matrix $\mathbf{Q}$, and a new generation $n+1$ takes place using the replaced entities. Here, $\mathcal{G}(\tilde{\Theta}_H)$ and $\mathcal{G}(\tilde{\Theta}_{S_{11}})$ denote the best individuals of the population associated with H and S_{11}, respectively, at the current generation n. In case at least one of the two stop conditions is satisfied, the best chromosome from the current first Pareto front is selected based on (9), which is implemented at the block of decision rules in Fig. 2. The selected chromosome is then decoded, yielding the final solution Θ^* that contains the information about the identified topology.

III. PROPOSED SPECIALIZATIONS OF THE GA ALGORITHM

This section describes the proposed schemes for GA coding/decoding, a novel algorithm for adapting the GA control parameters, and the utilization of the provided total line length (if used). The coding/decoding schemes are important to restrict the solution space to obtain a feasible solution. The algorithm for adapting the GA control parameters aims at improving the convergence of the optimization process. The approach for utilizing the line length handles the inherent uncertainty of the provided information.

A. Coding and Decoding

Coding/Decoding connects the chromosomes of the GA population with the line topology parameters in Θ and determines the search efficiency over the solution space. The schemes in this paper are described as follows.

1) Coding—The Constitution of the Chromosome: Each chromosome of the GA population has enough genes to store information about a line with N_s number of sections, where N_s is a user-defined parameter (see Table I). In particular, for each section, three genes represent the section length, the gauge, and the type (serial or bridged tap), respectively. For the first section, however, only two genes are needed, because the section is defined as serial in this paper. In addition, there are two genes for representing the effective number of bridged taps n_b and the effective number of sections n_s that the decoded chromosome (candidate line) will have. In summary, each chromosome is composed of $3N_s + 1$ number of genes, as illustrated in Fig. 3.

Each gene carries a real-valued number between 0 and 1. In the initialization, the values of the genes are randomly set

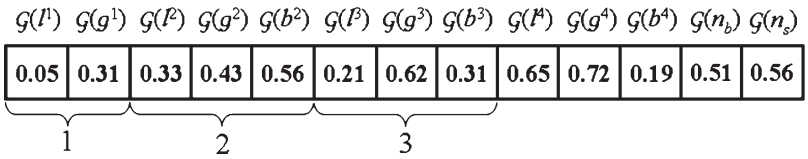

Fig. 3. Illustration of a chromosome with 13 genes ($N_s = 4$), with $n_s = 3$ effective numbers of sections.

following the uniform distribution $U[0, 1]$. During optimization, these values are optimized through the GA operators of selection, crossover, and mutation.

Recall that $\mathcal{G}^{-1}$ denotes the decoding from a gene to the corresponding element of Θ and that $\mathcal{G}$ denotes the coding of an element of Θ to the corresponding gene in the chromosome. This way, a coded x-gene of the sth line section of a certain line topology can be expressed as $\mathcal{G}(x^s)$, where $x \in \{l, g, b\}$. The next sections provide details of the decoding schemes for each kind of parameter in Θ, followed by a decoding example.

2) Decoding of the Number of Sections: The first gene that will be decoded in each chromosome is the gene that represents the effective number of sections, i.e., $\mathcal{G}(n_s)$. This case is essential because the decoded value of $\mathcal{G}(n_s)$, i.e., n_s, determines the remaining number of genes that will be decoded for the considered chromosome. In other words, in case $n_s < N_s$, only the genes that were associated with the first n_s sections are used to generate the candidate line topology. The remaining $N_s - n_s$ genes are not taken into account.

The decoding of the gene $\mathcal{G}(n_s)$ is essentially a mapping of the gene value to the integer value n_s. The adopted strategy consists of dividing the interval [0, 1] into $N_s - N_s^{\min} + 1$ equal subintervals, where $N_s^{\min}$ is the minimum number of sections, and N_s is the maximum number of sections (see Table I). Each subinterval is assigned one integer value within the range $[N_s^{\min}, N_s]$. That is, the first interval is assigned integer $N_s^{\min}$, the second interval is assigned integer $N_s^{\min} + 1$, and so on. Thus, the decoded value of the gene $\mathcal{G}(n_s)$ is equal to the integer that represents the subinterval in which the gene value falls. Typically, $N_s^{\min}$ is set to 1, because one-section lines are considered. However, if there is trustful a priori information about the number of sections of the line under test, then restrictions to $N_s^{\min}$ and N_s can be employed to reduce the search space.

The mapping of a real-valued gene to an integer through the aforementioned subintervals will be denoted in the following discussion by the operator $\mathcal{M}$, which is defined as

$$i = \mathcal{M}\left\{\mathcal{G}(x), [I_{\min}, I_{\max}]\right\} \tag{11}$$

where the gene $\mathcal{G}(x)$ is mapped to integer i that represents the subinterval within [0, 1], in which $\mathcal{G}(x)$ falls. In (11), $[I_{\min}, I_{\max}]$ denotes the interval of integers, where $I_{\min}$ and $I_{\max}$ are the lower and upper bounds, respectively. With this notation at hand, the decoding of the effective number of sections can be expressed as

$$n_s = \mathcal{M}\left\{\mathcal{G}(n_s), \left[N_s^{\min}, N_s\right]\right\}. \tag{12}$$

3) Decoding of Length and Gauge: The decoding of a gene into the corresponding section length involves the direct mapping of the gene value $\mathcal{G}(l^s) \in [0, 1]$ into the section length interval $[L_{\min}, L_{\max}]$. That is, for the sth section, the decoding of the length yields

$$l^s = L_{\min} + (L_{\max} - L_{\min})\mathcal{G}(l^s) \tag{13}$$

where $L_{\min}$ and $L_{\max}$ are user-defined parameters that set the minimum and maximum lengths of the section, respectively. The purpose of these bounds is to assure that the section lengths are within a feasible range. Typically, different length bounds are employed for serial and bridged-tap sections.

For the decoding of the genes related to the gauges, it is not feasible to employ a similar mapping as in (13), because the gauges are represented as discrete values. For example, the gauges of the European Telecommunications Standards Institute (ETSI) lines [22] are 0.32, 0.4, 0.5, 0.63, and 0.9 mm. To take this example into account, two different gauge-decoding algorithms, denoted *freegauge* and *gaugesort*, are considered in this paper.

As for the decoding of the number of sections, *freegauge* consists of dividing the gene interval [0, 1] into M equal subintervals, where M denotes the number of cable types in the assumed cable database. By applying the operator in (11), this decoding can be expressed as

$$i = \mathcal{M}\left\{\mathcal{G}(g^s), [1, M]\right\} \tag{14}$$

where $\mathcal{G}(g^s)$ denotes the considered gauge gene, and integer i denotes the ith element of the cable database. This way, assuming that the cable database is represented by the vector $\bar{G} = [G_1, \ldots, G_M]$, the decoded value of the gene $\mathcal{G}(g^s)$ is given by the ith position of the cable database, i.e.,

$$g^s = \bar{G}(i). \tag{15}$$

The *gaugesort* method is a more elaborate algorithm that aims at preventing the repetition of gauges along the line and assuring that the gauges are always increasing. That is, to decode each gauge gene, *gaugesort* takes into account the gauge of the previously decoded section and the number of remaining sections that will be decoded. In particular, at each decoding iteration, the number of available gauges for the decoding of a certain gauge gene $\mathcal{G}(g^s)$ is a subset of the assumed cable database, which is represented by the vector $\bar{G} = [G_1, \ldots, G_M]$. Algorithm 1 provides a formal description of the *gaugesort* algorithm, where i denotes the index of the previous used gauge, and s is the number of the line section under decoding. In each iteration, the integer interval $[i + 1, i + S]$ represents the indexes of the available gauges, in ascending order, and $(n_s - s)$ represents the number of remaining line sections that will be decoded. Note that *gaugesort* can only be used when the number of gauges in the cable database is larger than or equal to the effective number of sections n_s.

ALGORITHM 1: The *gaugesort* algorithm.

inputs: n_s, $\{\mathcal{G}(g^1), \ldots, \mathcal{G}(g^{n_s})\}$, $[G_1, \ldots, G_M]$
outputs: $\{g^1, \ldots, g^{n_s}\}$
$i = 0$;
$M = |\bar{G}|$;
for $s \leftarrow 1$ ***to*** n_s **do**
$S = M - i - (n_s - s)$;
$j = \mathcal{M}\{\mathcal{G}(g^s), [i+1, i+S]\}$;
$g^s = \bar{G}(j)$;
$i = j$;
end

4) Decoding of the Type of Sections: This decoding is equivalent to establishing whether a section is serial or a bridged tap. The procedure starts by determining the effective number of bridged taps n_b for each chromosome. By applying the operator in (11), the decoding of $\mathcal{G}(n_b)$ can be expressed as

$$n_b = \mathcal{M}\left\{\mathcal{G}(n_b), \left[N_b^{\min}, N_b\right]\right\} \tag{16}$$

where $N_b^{\min}$ is the user-defined minimum number of bridged taps. However, instead of being predefined, the maximum number of bridged taps N_b is determined from the effective number of sections n_s as follows:

$$N_b = \langle (n_s - 1)/2 \rangle \tag{17}$$

where $\langle \cdot \rangle$ refers to the round operation. Equation (17) reflects that the first section is defined as serial and that the bridged taps must alternate between serial sections along the path from the CO to the CP.

Having established the effective number of bridged taps $n_b > 0$, the next step is to determine the position of the bridged tap(s).

The first decoded bridged-tap position is found from at the index of the maximum type gene of the chromosome (i.e., a max search). In case $n_b > 1$, the position of the next bridged taps is found by iteratively performing max searches among the type genes but without taking into account the previously found type gene and its two neighboring genes. This way, the bridged taps alternate between serial sections. The decoding procedure is repeated until the n_b bridged taps are found.

5) Example of Decoding: A simple example shows how one can obtain the line parameters of Θ from the chromosome in Fig. 3. In this case, it is assumed that $N_s^{\min} = 1$, $N_s = 4$, and $N_b^{\min} = 0$.

First, the number of sections is decoded according to (12), with which the last gene $\mathcal{G}(n_s) = 0.56$ yields $n_s = 3$. Based on n_s, one obtains, using (16) and (17), $n_b = 1$. The position of the bridged tap is then determined according to the aforementioned max search, which gives that the bridged tap is located at the second section ($\mathcal{G}(b^2) = 0.56$).

By assuming that $L_{\min} = 100$ m and $L_{\max} = 4000$ m, the decoding of the length genes $\mathcal{G}(l^1)$, $\mathcal{G}(l^2)$, and $\mathcal{G}(l^3)$, using (13), yields $l^1 = 295$ m, $l^2 = 1387$ m and $l^3 = 919$ m.

For the decoding of the gauge genes, it is assumed that *freegauge* is employed with a cable database with 0.32, 0.4, 0.5, 0.63, and 0.9 mm. By applying (14) and (15), this approach results in $g^1 = 0.4$ mm, $g^2 = 0.5$ mm, and $g^3 = 0.63$ mm.

B. Self Adaptation of the GA Parameters

The two main parameters that control the GA process are the crossover probability p_c and the mutation probability p_m. Probability p_c controls the crossover, which determines if two chromosomes will exchange their genetic information to generate two new chromosomes. Probability p_m controls the mutation, which is applied to each gene of a chromosome, and determines whether the gene will suffer from mutation (modification). When a gene $\mathcal{G}(x)$ is selected to be modified, its new value $\mathcal{G}(x')$ is given by

$$\mathcal{G}(x') = \mathcal{G}(x) + \mathcal{N}(0, \sigma_m)$$

where $\mathcal{N}(0, \sigma_m)$ denotes a normal distribution with a mean that is equal to zero and a standard deviation of σ_m.

One general rule, which is widespread in the GA literature, is to use fixed (static) values for all parameters in the set $\Omega = \{p_c, p_m, \sigma_m\}$, which also include σ_m, which has an impact on the diversity of the GA population. In addition, the maximum number of generations N is usually kept constant throughout the optimization process. However, for line topology identification and other applications, this approach can be inefficient, and the algorithm may get stuck in local minima. Due to this case, a self-adaptive control algorithm is proposed to determine the values for N and the GA parameters in Ω along the optimization process.

The proposed strategy consists of sweeping the values of Ω, which were conditioned on the increase in the fitness[1] (*evolution* in GA terminology) of the best chromosomes. That is, the values of the GA parameters in Ω are maintained until they no longer provide evolution, whereupon they are changed. In addition, whenever any evolution of the fitness of the best chromosomes occur, the maximum number of generations N is increased, giving the algorithm more time to improve the candidate solutions.

One algorithm that implements this self adaptation is described in detail in Algorithm 2, where p_c^n, p_m^n, and σ_m^n are, respectively, the values of the crossover probability, mutation probability, and standard deviation at generation n. Here, P_c, P_m, and Σ_m are the maximum values of the crossover probability, mutation probability, and standard deviation, respectively (see Tables I and II). Variable c counts the number of consecutive generations without evolution, and δ_{p_c}, δ_{p_m}, and δ_{σ_m} indicate the decreasing rate of p_c, p_m, and σ_m, respectively.

ALGORITHM 2: Self-adaptive control algorithm for selecting the GA parameters.

Inputs: p_c^{n-1}, p_m^{n-1}, σ_m^{n-1}, δ_{p_c}, δ_{p_m}, and δ_{σ_m}
Outputs: p_c^n, p_m^n, and σ_m^n
for $n \leftarrow 1$ ***to*** N **do**
Calculate $\mathbf{Q}^n$ from Φ^n;
$\tilde{\Theta}_H^n = \arg\min_{r=1,2,\ldots R} V_H(\Theta_r^n)$;
$\tilde{\Theta}_{S_{11}}^n = \arg\min_{r=1,2,\ldots R} V_{S_{11}}(\Theta_r^n)$;

[1] *Fitness* is a figure or merit that is used in GA to classify the individuals of a population, and in this paper, its value will be the inverse of the value that was provided by the objective function.

if $V_H(\tilde{\Theta}_H^n) < V_H(\tilde{\Theta}_H)$ or $V_{S_{11}}(\tilde{\Theta}_{S_{11}}^n) < V_{S_{11}}(\tilde{\Theta}_{S_{11}})$ **then**
$N = N + \Delta N$;
$c = 0$;
else
$c = c + 1$;
end
if $c > w(N - n)$ **then**
$p_m^n = p_m^{n-1} - p_m^{n-1}\delta_{p_m}$;
$p_c^n = p_c^{n-1} - p_c^{n-1}\delta_{p_c}$;
$\sigma_m^n = \sigma_m^{n-1} - \sigma_m^{n-1}\delta_{\sigma_m}$;
$c = 0$
end
end

The algorithm can be summarized as follows. After calculating the objective matrix $\mathbf{Q}^n$ from the population Φ_n, at generation n, the best candidates $\tilde{\Theta}_H^n$ and $\tilde{\Theta}_{S_{11}}^n$ of the population have their values of the objective functions $V_H(\tilde{\Theta}_H^n)$ and $V_{S_{11}}(\tilde{\Theta}_{S_{11}}^n)$ compared with $V_H(\tilde{\Theta}_H)$ and $V_{S_{11}}(\tilde{\Theta}_{S_{11}})$, respectively. Here, $\tilde{\Theta}_H$ and $\tilde{\Theta}_{S_{11}}$ denote the current best candidates (see Table II). If any evolution in one of the current best GA solutions occurs, i.e., if $V_H(\tilde{\Theta}_H^n) < V_H(\tilde{\Theta}_H)$ or $V_{S_{11}}(\tilde{\Theta}_{S_{11}}^n) < V_{S_{11}}(\tilde{\Theta}_{S_{11}})$, variable c is reset to 0, and N is increased by ΔN. Otherwise, c is increased by 1.

Note from Algorithm 2 that the decision to change the values of $\Omega = \{p_c, p_m, \sigma_m\}$ is determined by $c > w(N - n)$, where c counts the number of consecutive generations without evolution, and $w(N - n)$ is a weighted number of remaining iterations. In particular, the difference $(N - n)$ defines the rate of change of the GA parameters. At the beginning of optimization, the difference $(N - n)$ is high, because n is low. This result means that a larger number of generations without evolution will be necessary to change the values in Ω. On the other hand, near the end of optimization, this difference is low, because n is almost equal to N. The rate of change of the values in Ω is therefore increased.

C. Utilization of the Total-Length Information

The objective of using the total length is to restrict the search space to improve the accuracy of the results and to improve the rate of convergence of the optimization process. The length information can be obtained, for example, from a line database or from the impulse response of the line under test, which was computed from the two-port measurements, i.e., using DELT.

The provided total line length can be considered fairly accurate but not error free. In particular, it is assumed in this paper that the provided length is accurate within $\pm 10\%$. That is, the total length is represented as a stochastic variable following the uniform distribution $U[0.9l, 1.1l]$, where l denotes the true line length. In case the GA uses this information as completely trustful, there will potentially be an intrinsic gap between the true topology and the best candidate of the GA population. This gap could occur, because the GA generates candidates with different topologies but with the same (static) total length. To handle this case, the total lengths of each candidate are fine tuned by the GA, as described in the following discussion.

One additional gene is included in each chromosome of the GA population. This gene stores a percentage value that was related to the uncertainty of the total length given to GA. Similar to other genes, the additional gene is tuned during optimization. The initial value E of this gene is generated according to the following formula:

$$E = E_{\min} + (E_{\max} - E_{\min})\alpha \tag{18}$$

where $E_{\min}$ and $E_{\max}$ are user-defined upper and lower bounds, and α is a chromosome-specific random number that was uniformly distributed at $U[0, 1]$. Under the given assumption of a total length uncertainty of $\pm 10\%$, it is natural to set $E_{\min}$ and $E_{\max}$ to be equal to $\pm 10\%$. However, to provide some extra freedom, we set $E_{\min} = -0.15$ and $E_{\max} = 0.15$, respectively. The percentage value E is used during decoding to calculate the total length $\hat{L}'_{\text{tot}}$ of each chromosome as follows:

$$\hat{L}'_{\text{tot}} = \hat{L}_{\text{tot}}(1 + E) \tag{19}$$

where $\hat{L}_{\text{tot}}$ is the length that was given to GA. The value of the obtained total length $\hat{L}'_{\text{tot}}$ of each chromosome is then divided among the serial sections of the line, taking into account the genes that were associated with the section lengths, as follows:

$$l^s = \hat{L}'_{\text{tot}} \frac{\mathcal{G}(l^s)}{\mathcal{G}(l^1) + G(l^2) + \cdots + \mathcal{G}(l^{n_s})}. \tag{20}$$

IV. Simulation Results

This section presents simulation results to validate the proposed method, i.e., TIMEC. Here, instead of actually measuring $\hat{H}$ and $\hat{S}_{11}$ for a given line under test, these quantities are obtained using the operator $\mathcal{V}$ in (6), which employs a cable model, as described in Section II-A. In other words, the correct set of parameters $\Theta^\dagger$ is used to generate the target functions, and consequently, $\hat{H} = H^\dagger$, and $\hat{S}_{11} = S_{11}^\dagger$. The same cable model is also used to generate the quantities that were associated with the candidates of the population. Under these controlled conditions, there are no measurement or modeling mismatches (see Appendix A). This way, it is feasible to exactly find $\Theta^* = \Theta^\dagger$. In addition, there is no uncertainty that was associated with the generation of the quantities, and hence, the variances in (7) and (8) are set to 1.

A. General Simulation Conditions

The simulations are organized according to the amount of available information, as defined in Table III. The aim is to investigate the performance of TIMEC based on either one-port measurements or both one- and two-port measurements and to further employ information about the (total) line length. TIMEC is evaluated for each of the four *test cases* in Table III. For Test Cases 1 and 2, TIMEC is compared with a reference method based on only one-port measurements, denoted SELT-tdr. For Test Cases 3 and 4, TIMEC is evaluated with different degrees of accuracy in the line length information.

TABLE III
SUMMARY OF THE EMPLOYED TEST CASES AND THEIR RESPECTIVE RESULT TABLES

Method	Test Case	Available Information				Result Table
		One-port meas.	Two-port meas.	Total length (±10%)	True total length	
SELT-tdr		x				V and VI
TIMEC	1	x				V
	2	x	x			VI
	3	x	x	x		VII
	4	x	x		x	VIII

TABLE IV
UPPER AND LOWER BOUNDS FOR THE LINE PARAMETERS

Parameter	Bounds	
	lower	upper
Serial section length (km)	$L_{\min} = 0.02$	$L_{\max} = 7$
Bridged-tap section length (km)	$L_{\min} = 0.05$	$L_{\max} = 0.8$
Number of sections	$N_s^{\min} = 1$	$N_s = 5$
Number of bridged-taps	$N_b^{\min} = 0$	$N_b = 2$

A comprehensive set of eight *test lines* is used for each test case. The selected test lines are ETSI #4, #5, #6, #7, and #8, as defined in [22], two test lines that were defined in [8], which are here called Loops G#1 and G#2, and one test line that was defined in [4], here called SBTS. These test lines (i.e., their topology) are described in Tables V–VIII. All the test lines have an open-end termination at the remote side. The VUB [18] cable model, with the restrictions described in Appendix B, is used to generate the quantities of interest during the simulations using (6). The considered frequency band corresponds to the case of ADSL with 256 tones, which range from 4.3125 kHz to 1.104 MHz.

The proposed method is based on GA, i.e., stochastic optimization; thus, it is important to determine the statistics of the estimated section lengths for independent simulations. TIMEC is therefore applied ten times for each test line and test case, and each estimated section length is presented in the following result tables with its mean value and standard deviation.

The employed GA uses the self-adaptive control algorithm in Section III-B, and the bounds for the line parameters are set as shown in Table IV.

The internal GA configuration is described as follows. The population size R is set to 30, the maximum crossover probability is set to $P_c = 0.85$, the maximum mutation probability is set to $P_m = 0.85$, and the maximum standard deviation of mutation is set to $\Sigma_m = 0.75$. The threshold δ for the sum of the objective functions is set to 10^{-7}. These values were determined from empirical experiments, which provide a tradeoff between the accuracy and rate of convergence and are suitable for the test cases in this paper. In addition, $\Delta N = 50$, w is equal to 0.05, δ_{p_c} and δ_{p_m} are set to 0.005, and δ_{σ_m} is set to 0.01.

The usage of the decoding algorithms *gaugesort* and *freegauge*, as described in Section III-A3, is given as follows. TIMEC uses as default the *freegauge*. In case that no bridged taps are detected, TIMEC is executed with *gaugesort* to improve the accuracy.

B. TIMEC for Test Cases 1 and 2

This section presents a comparison between TIMEC and the state-of-the-art TDR-based reference method in [4], here denoted as *SELT-tdr*. In particular, TIMEC for Test Cases 1 and 2 in Table III is compared with SELT-tdr for all eight test lines. Before presenting the test results, the reference method is briefly described.

The TDR-based method in [4] was selected, because it has documented good results for different line topologies, as described in [8, Table II, pp. 545]. For this paper, the method was implemented by strictly following the process in [4], except for the technique for detecting singularities in the so-called reflectogram [4]. This case is unfortunately not described in [4]. We therefore employ derivatives to detect those singularities. Our implementation of SELT-tdr was tested with the lines in [8], obtaining similar results as the reported ones. It is also worth mentioning that our implementation uses a velocity of propagation set to 68.7% of the speed of light in vacuum, which was calculated according to the description in [4].

1) Test Case 1—TIMEC Based on One-Port Measurements: The results for this test case are summarized in Table V, which shows the estimated length and the percentage error $\Delta l(\%)$ of the sections for SELT-tdr. For TIMEC, the mean estimated length, the mean percentage error $\overline{\Delta l(\%)}$, and the standard deviation σ for each section, calculated from ten independent simulations, are given. For all result tables, the estimated lengths are rounded to integer values, $\Delta l(\%)$ and $\overline{\Delta l(\%)}$ are rounded to two decimals, and σ is rounded to four decimals.

The results that were provided by the SELT-tdr method highlight two main features of such a method: it is well suited for detecting bridged taps but is not successful in detecting all kinds of gauge changes. A gauge change constitutes an impedance change that is often small in comparison to, for example, the impedance change due to a bridged tap. Some gauge changes yield a more prominent reflection coefficient than others, as shown in Fig. 4, where the magnitude of the reflection coefficients for all gauge changes in the considered test lines are plotted as a function of frequency. It is shown that, in particular, the gauge changes 0.32/0.4 mm, 0.32/0.5 mm, and 0.5/0.9 mm provide large impedance changes for a broad frequency range. Consequently, these gauge changes are easier to detect. This result is confirmed for ETSI #7, which has two large impedance changes (0.32/0.5 mm and 0.5/0.9 mm). The results in Table V show that the line topology of ETSI #7 is correctly detected with SELT-tdr, except for the gauge type of the second section. In Fig. 4, it can also be observed that the gauge changes 0.5/0.63 mm and 0.63/0.9 mm have the lowest impedance changes. The latter gauge change is reflected in the results of SELT-tdr for ESTI #4, #5, and #6, where only one or

TABLE V
RESULTS FOR TEST CASE 1: COMPARISON BETWEEN SELT-tdr [4] AND TIMEC USING ONLY ONE OBJECTIVE FUNCTION BASED ON S_{11}

Actual Topology				Estimated Topology - SELT-tdr				Estimated Topology - TIMEC (S_{11})				
Loop	Type	Gauge (mm)	Length (m)	Type	Gauge (mm)	Length (m)	Δl (%)	Type	Gauge (mm)	Mean Length (m)	$\overline{\Delta l}$ (%)	σ (m)
Loop G#1	Serial	0.40	164	Serial	0.40	151.70	7.50	Serial	0.40	164.05	0.05	0.0002
Loop G#2	Serial	0.50	195	Serial	0.50	195.02	0.01	Serial	0.50	195.06	0.01	0.0000
ETSI#4	Serial	0.32	200	Serial	0.32	216.70	8.35	Serial	0.32	200.00	0.00	0.0000
	Serial	0.40	900	Serial	0.40	2535.20	181.69	Serial	0.40	899.80	0.04	0.0005
	Serial	0.50	1500	Serial	–	–	–	Serial	0.50	1986.40	32.43	0.0010
	Serial	0.63	500	Serial	–	–	–	–	–	–	–	–
ETSI#5	Serial	0.40	1450	Serial	0.40	2361.90	62.89	Serial	0.40	1447.50	0.17	0.0011
	Serial	0.50	750	–	–	–	–	Serial	0.50	947.10	26.28	0.0050
	Serial	0.63	500	–	–	–	–	Serial	0.90	800.03	60.01	0.0048
	Serial	0.90	500	–	–	–	–	–	–	–	–	–
ETSI#6	Serial	0.40	1300	Serial	0.40	2663.70	104.90	Serial	0.40	1299.30	0.05	0.0001
	Serial	0.50	1250	–	–	–	–	Serial	0.50	1736.40	38.90	0.0003
	Serial	0.63	500	–	–	–	–	–	–	–	–	–
ETSI#7	Serial	0.32	200	Serial	0.32	216.70	8.35	Serial	0.32	200.03	0.03	0.0001
	Serial	0.50	600	Serial	0.40	671.70	11.95	Serial	0.40	599.80	0.07	0.0005
	Serial	0.90	4000	Serial	0.90	3098.6	22.54	Serial	0.90	4000.80	0.04	0.0023
ETSI#8	Serial	0.40	750	Serial	0.40	736.70	1.77	Serial	0.40	749.98	0.01	0.0001
	BT	0.40	500	BT	0.40	108.30	78.34	BT	0.40	500.06	0.07	0.0003
	Serial	0.40	1100	Serial	0.63	390.90	64.55	Serial	0.40	1601.40	45.58	0.0020
	BT	0.40	500	BT	0.40	86.60	477.4	–	–	–	–	–
SBTS	Serial	0.50	300	Serial	0.50	303.20	1.07	Serial	0.50	300.20	0.07	0.0003
	BT	0.50	300	BT	0.50	303.20	1.07	BT	0.50	299.80	0.08	0.0003
	Serial	0.50	900	Serial	0.50	909.50	1.06	Serial	0.50	899.80	0.02	0.0002

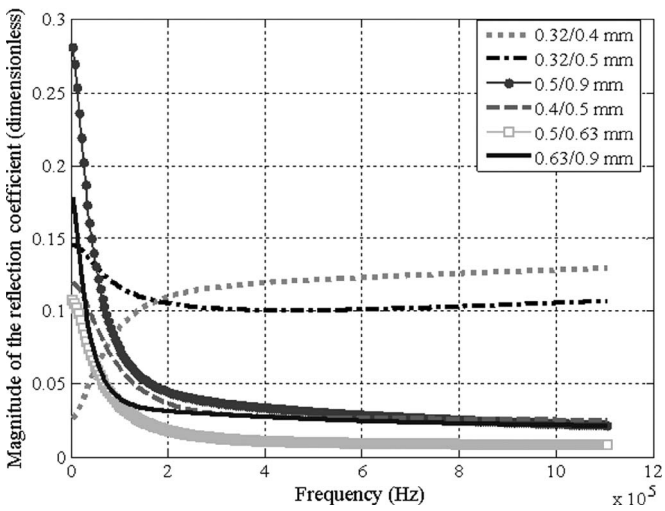

Fig. 4. Magnitude of the reflection coefficients as a function of frequency, which is related to all impedance mismatches in the considered test lines.

two serial sections are detected, with an estimation error on the total length of about 26%, 13%, and 4%, respectively. Note that the total length estimations are not shown in the result table(s) but can be calculated as a sum of the estimated section lengths. For the one-section lines, i.e., Loops G #1 and G #2, SELT-tdr has an error on the total length estimates below 8%.

For TIMEC, the results in Table V show that the estimation errors are negligible for Loop G #1, Loop G #2, and SBTS. The last sections of ETSI #4, #5, #6, and #8 are not detected, but the percentage error of length for the first section(s) of these lines is small. In addition, for these lines, the estimated length of the last detected section is almost equal to the sum of the two last sections of the true line, yielding a mean estimate of the total length less than 0.5%. For ETSI #7, the TIMEC results are accurate with a mean percentage error of the section lengths less than 0.1%.

In summary, Table V indicates that the results that were provided by TIMEC, using only one-port measurements with one objective function, are equal to or better than those provided by the SELT-tdr method. For lines with incorrectly detected topologies, TIMEC provides an accurate estimate of the first section(s) and the total line length. For both methods, test lines that contain small impedance changes prove to be more difficult to estimate. The standard deviations in Table V are all small, indicating that the same (local) optimum is found

TABLE VI
RESULTS FOR TEST CASE 2: COMPARISON BETWEEN SELT-tdr [4] AND TIMEC USING TWO OBJECTIVE FUNCTIONS BASED ON S_{11} AND H

Actual Topology				Estimated Topology - SELT-tdr				Estimated Topology - TIMEC (S_{11},H)				
Loop	Type	Gauge (mm)	Length (m)	Type	Gauge (mm)	Length (m)	Δl (%)	Type	Gauge (mm)	Mean Length (m)	$\overline{\Delta l}$ (%)	σ (m)
Loop G#1	Serial	0.40	164	Serial	0.40	151.70	7.50	Serial	0.40	164.00	0.03	0.0001
Loop G#2	Serial	0.50	195	Serial	0.50	195.02	0.01	Serial	0.50	195.02	0.03	0.0001
ETSI# 4	Serial	0.32	200	Serial	0.32	216.70	8.35	Serial	0.32	200.00	0.00	0.0000
	Serial	0.40	900	Serial	0.40	2535.20	181.69	Serial	0.40	900.00	0.00	0.0000
	Serial	0.50	1500	Serial	–	–	–	Serial	0.50	1563.00	4.20	0.0763
	Serial	0.63	500	Serial	–	–	–	Serial	0.63	404.00	19.20	0.1109
ETSI# 5	Serial	0.40	1450	Serial	0.40	2361.90	62.89	Serial	0.40	1450.00	0.00	0.0000
	Serial	0.50	750	–	–	–	–	Serial	0.50	925.00	23.60	0.0854
	Serial	0.63	500	–	–	–	–	Serial	0.63	769.00	55.00	0.1354
	Serial	0.90	500	–	–	–	–	–	–	–	–	–
ETSI# 6	Serial	0.40	1300	Serial	0.40	2663.70	104.90	Serial	0.40	1300.00	0.00	0.0000
	Serial	0.50	1250	–	–	–	–	Serial	0.50	1401.00	12.24	0.1072
	Serial	0.63	500	–	–	–	–	Serial	0.90	387.00	23.00	0.1120
ETSI# 7	Serial	0.32	200	Serial	0.32	216.70	8.35	Serial	0.32	200.00	0.00	0.0000
	Serial	0.50	600	Serial	0.40	671.70	11.95	Serial	0.50	600.00	0.00	0.0000
	Serial	0.90	4000	Serial	0.90	3098.60	22.54	Serial	0.90	4000.00	0.00	0.0000
ETSI# 8	Serial	0.40	750	Serial	0.40	736.70	1.77	Serial	0.40	750.00	0.00	0.0000
	BT	0.40	500	BT	0.40	108.30	78.34	BT	0.40	500.00	0.00	0.0000
	Serial	0.40	1100	Serial	0.63	390.00	64.55	Serial	0.40	1100.00	0.00	0.0000
	BT	0.40	500	BT	0.40	86.60	477.4	BT	0.40	500.00	0.00	0.0000
SBTS	Serial	0.50	300	Serial	0.50	303.20	1.07	Serial	0.50	300.10	0.03	0.0000
	BT	0.50	300	BT	0.50	303.20	1.07	BT	0.50	300.10	0.04	0.0000
	Serial	0.50	900	Serial	0.50	909.50	1.06	Serial	0.50	900.20	0.02	0.0000

for the repeated trials with TIMEC. Furthermore, in case only one-port measurements are used with a priori information about the total line length (not previously described), no significant improvements can be observed with TIMEC.

2) Test Case 2—TIMEC Based on Both One- and Two-Port Measurements: The results with TIMEC for Test Case 2 are listed in Table VI, where the SELT-tdr results for Test Case 1 are repeated for convenience.

Here, two objective functions based on both one- and two-port measurements are used by TIMEC. Based on Table VI, we note that the number of line sections for all test lines are correctly estimated with TIMEC, except for ETSI #5. A perfect topology estimation is obtained for ETSI #8, where the bridged taps are found at their correct positions, i.e., at the second and fourth line sections. For ETSI #4, the length of the third and fourth line sections are somewhat *overestimated* and *underestimated*, respectively, yielding a mean percentage error of a total length of 2.0%. For ETSI #5, the last line section is not detected, but the mean percentage error of the total length is only 1.3%. For ETSI #6, the gauge of the last line section is incorrectly estimated, and the mean percentage error of the total length is 1.24%.

In summary, TIMEC based on both one- and two-port measurements improves the estimation results compared to using only one-port measurements, as expected. As for Test Case 1, the estimation of the last section(s) fails for lines with small impedance changes, although the mean percentage error of the total length is small. The standard deviations for TIMEC with repeated trials are small or zero, except for the last section of ETSI #5, indicating that the same (local) optimum is found.

C. TIMEC for Test Cases 3 and 4

This section presents the performance results of TIMEC using two objective functions based on one- and two-port measurements and a measure of the total line length.

1) Test Case 3—Inaccurate Total-Length Information: For this test case, TIMEC is provided with the total length of each test line, which was offset by $+10\%$ relative the total length. That is, the provided input to the TIMEC is $1.1l$ m for a line with a total length of l m. To handle this case, TIMEC uses the approach and associated settings in Section III-C.

The results for this test case are shown in Table VII, which shows that the topological structures (number of sections,

TABLE VII
RESULTS FOR TEST CASE 3: TIMEC USING TWO OBJECTIVE FUNCTIONS, WHICH WERE BASED ON S_{11} AND H, AND THE TOTAL LENGTH VALUE WITH A +10% OFFSET

Actual Topology				Estimated Topology - TIMEC (S_{11},H)				
Loop	Type	Gauge (mm)	Length (m)	Type	Gauge (mm)	Mean Length (m)	$\overline{\Delta l}$ (%)	σ (m)
Loop G#1	Serial	0.40	164	Serial	0.40	163.98	0.00	0.0000
Loop G#2	Serial	0.50	195	Serial	0.50	195.07	0.00	0.0000
ETSI#4	Serial	0.32	200	Serial	0.32	200.00	0.05	0.0002
	Serial	0.40	900	Serial	0.40	904.59	1.36	0.0124
	Serial	0.50	1500	Serial	0.50	1486.10	2.06	0.0300
	Serial	0.63	500	Serial	0.63	509.10	3.88	0.0207
ETSI#5	Serial	0.40	1450	Serial	0.40	1449.26	0.24	0.0047
	Serial	0.50	750	Serial	0.50	752.11	0.91	0.0086
	Serial	0.63	500	Serial	0.63	497.31	1.91	0.0113
	Serial	0.90	500	Serial	0.90	501.45	1.31	0.0073
ETSI#6	Serial	0.40	1300	Serial	0.40	1301.74	0.29	0.0042
	Serial	0.50	1250	Serial	0.50	1244.19	0.85	0.0107
	Serial	0.63	500	Serial	0.63	502.78	1.45	0.0074
ETSI#7	Serial	0.32	200	Serial	0.32	200.03	0.04	0.0001
	Serial	0.40	600	Serial	0.40	599.89	0.21	0.0014
	Serial	0.90	4000	Serial	0.90	3999.84	0.04	0.0019
ETSI#8	Serial	0.40	750	Serial	0.40	750.30	0.05	0.0007
	BT	0.40	500	BT	0.40	499.90	0.22	0.0016
	Serial	0.40	1100	Serial	0.40	1099.80	0.06	0.0009
	BT	0.40	500	BT	0.40	499.30	0.23	0.0019
SBTS	Serial	0.50	300	Serial	0.50	300.00	0.01	0.0000
	BT	0.50	300	BT	0.50	299.97	0.02	0.0001
	Serial	0.50	900	Serial	0.50	900.00	0.00	0.0000

section types, and gauges) of all considered lines are accurately detected by TIMEC. In particular, the topology identification of ETSI #5 has significantly been improved compared to previous test cases. The mean error on the total length estimation is negligible (i.e., $< 0.1\%$) for all test lines, which means that TIMEC can fine tune the provided (erroneously) total length values.

2) Test Case 4—Perfect Total-Length Information: For Test Case 4, the total length information is assumed to be free of error. In this case, GA considers the length information as trustful, i.e., the approach in Section III-C is not employed. In other words, unlike in Test Case 3, all candidate lines that were generated during optimization have the same total length, which was equal to the given value.

As indicated in Table VIII, the results are slightly better than for Test Cases 1 and 2. As for Test Case 3, the topological structure is accurately detected by TIMEC for all considered lines. However, note from Table VIII that, for some of the lines, the mean percentage error of the section lengths is somewhat increased compared to Test Case 3.

V. SUMMARY AND CONCLUSION

This paper has presented a new method for line topology identification. The proposed model-based method, called TIMEC, takes advantage of both conventional one-port measurements S_{11} and two-port measurements (transfer function). The latter measurement is obtained using the line-diagnostic functionality in the ITU-T G.992.3 and G.992.5 Standards. These measurement quantities are used in two objective functions that are optimized with NSGA-II. In addition, specialized schemes for coding/decoding are adopted together with an algorithm for self adaptation of the GA parameters.

One important property of the chosen GA-based approach is its flexibility, which permits the incorporation of additional measurements or a priori line information, e.g., the total line length. Although the TIMEC method based on only one-port S_{11} measurements utilizes the same information as the SELT-tdr method, it performs slightly better. By also including the two-port measurements (transfer function), the difference in performance between TIMEC and SELT-tdr is considerably increased. Finally, when information about the total line length

TABLE VIII
RESULTS FOR TEST CASE 4: TIMEC USING TWO OBJECTIVE FUNCTIONS, WHICH WERE BASED ON S_{11} AND H, AND THE TOTAL LENGTH VALUE

Actual Topology				Estimated Topology - TIMEC (S_{11},H)				
Loop	**Type**	**Gauge (mm)**	**Length (m)**	**Type**	**Gauge (mm)**	**Mean Length (m)**	$\overline{\Delta l}$ **(%)**	σ **(m)**
Loop G#1	Serial	0.40	164	Serial	0.40	163.98	0.00	0.0000
Loop G#2	Serial	0.50	195	Serial	0.50	195.07	0.00	0.0000
ETSI#4	Serial	0.32	200	Serial	0.32	200.00	0.00	0.0000
	Serial	0.40	900	Serial	0.40	900.00	0.00	0.0000
	Serial	0.50	1500	Serial	0.50	1524.00	2.13	0.0470
	Serial	0.63	500	Serial	0.63	476.00	6.40	0.1010
ETSI#5	Serial	0.40	1450	Serial	0.40	1450.00	0.00	0.0000
	Serial	0.50	750	Serial	0.50	754.00	1.33	0.0092
	Serial	0.63	500	Serial	0.63	495.00	4.20	0.0300
	Serial	0.90	500	Serial	0.90	503.00	3.00	0.0161
ETSI#6	Serial	0.40	1300	Serial	0.40	1300.00	0.00	0.0000
	Serial	0.50	1250	Serial	0.50	1270.00	1.60	0.0600
	Serial	0.63	500	Serial	0.63	487.00	2.60	0.0390
ETSI#7	Serial	0.32	200	Serial	0.32	200.00	0.00	0.0000
	Serial	0.40	600	Serial	0.40	598.00	0.33	0.0040
	Serial	0.90	4000	Serial	0.90	3996.00	0.10	0.0092
ETSI#8	Serial	0.40	750	Serial	0.40	750.00	0.00	0.0000
	BT	0.40	500	BT	0.40	500.00	0.00	0.0000
	Serial	0.40	1100	Serial	0.40	1100.00	0.00	0.0000
	BT	0.40	500	BT	0.40	500.00	0.00	0.0000
SBTS	Serial	0.50	300	Serial	0.50	300.04	0.04	0.0002
	BT	0.50	300	BT	0.50	299.77	0.09	0.0002
	Serial	0.50	900	Serial	0.50	899.98	0.02	0.0003

is included, the TIMEC method correctly determines all considered test-line topologies in terms of the number of sections, types, gauges, and lengths.

APPENDIX A

This appendix tries to clearly distinguish the sources of errors in the proposed model-based analysis-by-synthesis method.

Assuming that $\hat{H}$ is a measured quantity (the same reasoning is valid for $\hat{S}_{11}$), one wants to find a line Θ with minimum error Δ_v, where

$$H = \mathcal{V}\{\Theta\} = \hat{H} + \Delta_v.$$

The error Δ_v can be decomposed into the parcels

$$\Delta_v = \Delta_v^n + \Delta_v^m + \Delta_v^t + \Delta_v^s + \Delta_v^p$$

which can be summarized as follows.

1) Statistical measurement errors Δ_v^n: errors due to internal measurement noise, e.g., thermal noise and external noise as RF interference. These types of noise can normally be suppressed by averaging.
2) Systematic measurement errors Δ_v^m: errors due to an imperfect measurement setup and calibration procedure.
3) Topology error Δ_v^t: error due to an incorrect topology assumption, i.e., when Θ is not the correct $\Theta^\dagger$.
4) Structural error Δ_v^s: error due to a bad choice of the cable model. For example, a VUB cable model cannot fully describe a BT-modeled line.
5) Parameter error Δ_v^p: error due to the imperfect translation of line gauge into the cable model parameters. For example, two cables of the same diameter could have a difference in one or more of the other model parameters.

Parcels Δ_v^n and Δ_v^m are not relevant in this paper, because simulated measurement data are used. Moreover, Δ_v^p is zero, because the cable database in Appendix B is used for the simulated measurement data and is employed by TIMEC. On the other hand, parcels Δ_v^t and Δ_v^s exist because of the adopted model-based approach and deserve further discussion. For example, the BT #1 cable model [19] provides a result $H = \mathcal{V}_{\mathrm{BT}}(\Theta)$ based on a set Λ_{BT} with $|\Lambda_{\mathrm{BT}}| = 13$ parameters.

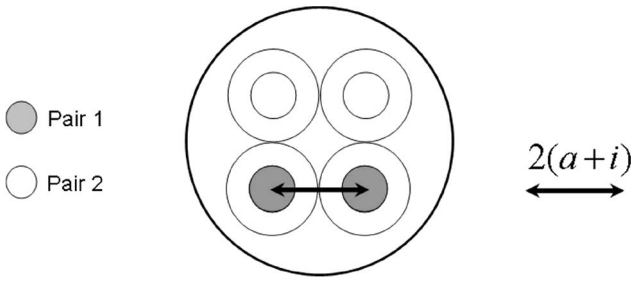

Fig. 5. Distance between the center of the conductors for a twisted pair structure.

Assuming that the other parcels are zero, i.e., $\Delta_v^n = \Delta_v^m = \Delta_v^t = \Delta_v^p = 0$, and a cable model provides Λ, Δ_v^s is defined as the error $\Delta_v^s = \arg\min_\Lambda V(\Theta(\Lambda))$, where the dependence on Λ is made explicit in $\Theta(\Lambda)$ for readability, and $V(\Theta(\Lambda))$ is given by (7). In other words, if one assumes the BT model, Δ_v^s should be obtained by trying all possible (an infinite number) sets $\Lambda_{\rm BT} \in \mathbb{C}^{|\Lambda_{\rm BT}|}$. This error is called structural, because $\Delta_v^s \neq 0$ means that the model cannot fit the measured $\hat{H}$, even after trying all possible combinations of parameters with $\Delta_v^t = \Delta_v^n = \Delta_v^m = 0$.

One may account for the total $\Delta_v^t + \Delta_v^s + \Delta_v^p$ but cannot individually estimate each parcel. In simulations, however, all these parcels can be accounted for. This approach is a motivation for starting the validation of the proposed TIMEC method from a well-controlled simulation setup, where $\Delta_v^s = \Delta_v^p = \Delta_v^n = \Delta_v^m = 0$, and the only error is Δ_v^t, i.e., the topology error.

APPENDIX B

This appendix presents the values of the geometrical and electromagnetic parameters that were adopted for the VUB cable model in this paper.

The VUB model is based on geometrical assumptions and models the propagation constant and characteristic impedance (γ and Z_0) of a cable by using parameterized equations. These equations are stated as a function of parameters, here called the VUB parameters. These parameters, in turn, depend on geometrical and electromagnetic parameters that were associated with the conductor and the insulation materials. The geometrical parameters are given as follows: 1) the radius of the conductors a; 2) the insulation thickness of the conductor i; and 3) the distance from the center of the conductors D. The electromagnetic parameters are given as follows: 1) the relative permeability μ_r of the insulation; 2) the relative permittivity ϵ_r of the insulation; and 3) the conductor conductivity σ. It is assumed that the insulation material is polyethylene, the conductor material is copper, and the cables are structured as twisted pairs. The values for a, i, σ, μ_r, and ϵ_r are based on [22].

The way that the cables is structured determines the calculation of the variable D, as illustrated in Fig. 5. For a twisted-pair-structured cable of certain gauge g, D is expressed by

$$D = 2\left(a(g) + i(g)\right).$$

TABLE IX
GEOMETRICAL AND ELECTROMAGNETIC PARAMETERS FOR THE CONSIDERED CABLE TYPES, WHICH WERE ADOPTED FOR THE VUB CABLE MODEL IN THE SIMULATIONS

Parameters	0.32 mm	0.4 mm	0.5 mm	0.63 mm	0.9 mm
$a\ (mm)$	0.16	0.2	0.25	0.315	0.45
$i\ (mm)$	0.05	0.13	0.15	0.2	0.27
$D\ (mm)$	0.42	0.66	0.8	1.03	1.44
$\sigma\ (S/m)$	5.8×10^7				
μ_r	1				
ϵ_r	2.26				

Table IX summarizes the values for the geometrical and electromagnetic parameters associated with a certain diameter, which were adopted for the VUB cable model in the simulations.

REFERENCES

[1] T. Starr, J. M. Cioffi, and P. J. Silverman, *Understanding Digital Subscriber Line Technology*. Englewood Cliffs, NJ: Prentice-Hall, 1999.
[2] S. Galli and D. L. Waring, "Loop makeup identification via single-ended testing: Beyond mere loop qualification," *IEEE J. Sel. Areas Commun.*, vol. 20, no. 5, pp. 923–935, Jun. 2002.
[3] J. L. Fang, C. Zeng, and J. Cioffi, *Bridged-tap location estimation*. preprint.
[4] S. Galli and K. J. Kerpez, "Single-ended loop makeup identification—Part I: A method of analyzing TDR measurements," *IEEE Trans. Instrum. Meas.*, vol. 55, no. 2, pp. 528–537, Apr. 2006.
[5] P. Boets, T. Bostoen, L. Van Biesen, and T. Pollet, "Preprocessing of signals for single-ended subscriber-line testing," *IEEE Trans. Instrum. Meas.*, vol. 55, no. 5, pp. 1509–1518, Oct. 2006.
[6] J. R. i Riu, "Position paper on loop qualification and monitoring (Outlining general features the developed loop qualification and monitoring solution should fulfill)," Ericsson AB, Stockholm, Sweden, Nov. 2004. Report.
[7] G. Long and J. Kamali, "Single-ended line probing helps speed up DSL mass deployment," in *Proc. IIC-China/ESC China Conf.*, 2002, pp. 57–60.
[8] K. J. Kerpez and S. Galli, "Single-ended loop-makeup identification—Part II: Improved algorithms and performance results," *IEEE Trans. Instrum. Meas.*, vol. 55, no. 2, pp. 538–549, Apr. 2006.
[9] T. Vermeiren, T. Bostoen, P. Boets, X. Ochoa Chebab, and F. Louage, "Subscriber loop topology classification by means of time-domain reflectometry," in *Proc. IEEE ICC*, May 2003, vol. 3, pp. 1998–2002.
[10] C. Neus, P. Boets, and L. Van Biesen, "Feature extraction of one-port scattering parameters for single-ended line testing," in *Proc. XVIII IMEKO World Congr.*, 2006.
[11] *Asymmetric Digital Subscriber Line Transceivers 2 (ADSL2)*, ITU-T recommendation G.992.3, Jan. 2005.
[12] *Asymmetric Digital Subscriber Line (ADSL) Transceivers: Extended Bandwidth ADSL2 (ADSL2+)*, ITU-T recommendation G.992.5, Jan. 2005.
[13] K. Deb, A. Pratap, S. Agarwal, and T. Meyarivan, "A fast and elitist multiobjective genetic algorithm: NSGA-II," *IEEE Trans. Evol. Comput.*, vol. 6, no. 2, pp. 182–197, Apr. 2002.
[14] K. Deb, *Multiobjective Optimization Using Evolutionary Algorithms*. Hoboken, NJ: Wiley, 2001.
[15] G. N. Beligiannis, L. V. Skarlas, and S. D. Likothanassis, "A generic applied evolutionary hybrid technique for adaptive system modeling and information mining," *IEEE Signal Process. Mag.*, vol. 21, no. 3, pp. 28–38, May 2004.
[16] G. N. Beligiannis, L. V. Skarlas, S. D. Likothanassis, and K. Perdikouri, "Nonlinear model structure identification of complex biomedical data using a genetic-programming-based technique," *IEEE Trans. Instrum. Meas.*, vol. 54, no. 6, pp. 2184–2190, Dec. 2005.
[17] P. Golden and J. Cook, "The copper channel: Loop characteristics and models," in *Fundamentals of DSL Technology*. New York: Auerbach, 2006, ch. 2.

[18] P. Boets, M. Zekri, L. Van Biesen, T. Bostoen, and T. Pollet, "On the identification of cables for metallic access networks," in *Proc. 18th IEEE IMTC*, May 2001, vol. 2, pp. 1348–1353.
[19] R. van den Brink, *Cable reference models for simulating metallic access networks*, 1998. ETSI STC. TM6.
[20] F. Lindqvist, P. Börjesson, P. Ödling, S. Höst, K. Ericson, and T. Magesacher, "Low-order and causal twisted-pair cable modeling by means of the Hilbert transform," in *Proc. 20th Nordic Conf. Radio Sci. Commun.: RVK*, Växjö, Sweden, Jun. 9–11, 2008, pp. 301–310.
[21] T. Bostoen, P. Boets, M. Zekri, L. Van Biesen, T. Pollet, and D. Rabijns, "Estimation of the transfer function of a subscriber loop by means of a one-port scattering parameter measurement at the central office," *IEEE J. Sel. Areas Commun.*, vol. 20, no. 5, pp. 936–948, Jun. 2002.
[22] *Test Procedures for Digital Subscriber Line (DSL) Transceivers*, ITU-T recommendation G.996.1, Feb. 2001.

Claudomiro Sales received the M.Sc. degree in electrical engineering in 2005 from the Federal University of Para, Belem, Brazil, where he is currently working toward the Ph.D. degree in the Institute of Technology.

His research interests include genetic algorithms, optimization techniques, measurements, and system identification. His current research work is focused on loop identification using double-ended line testing for xDSL systems and multiobjective genetic algorithms.

Roberto M. Rodrigues received the M.Sc. degree in electrical engineering in 2005 from the Federal University of Para, Belem, Brazil, where he is currently working toward the Ph.D. degree in the Institute of Technology.

His research interests include the frequency-domain identification of transmission lines, measurement systems, optimization techniques, and simulation systems.

Fredrik Lindqvist received the M.Sc. degree in electrical engineering from the Royal Institute of Technology (KTH), Stockholm, Sweden, in 1999. He is currently working toward the Ph.D. degree in the Department of Electrical and Information Technology, Lund University, Lund, Sweden.

From 1999 to 2006, he was a Research Engineer with the DSL Access Signal Processing Laboratory, Ericsson A.B., Stockholm. Since 2006, he has been working on signal processing algorithms and performance analysis for wireless systems with Ericsson A.B.

João Costa (S'94–M'95) received the B.Sc. degree in electrical engineering from the Federal University of Para (UFPA), Belem, Brazil, in 1981, the M.Sc. degree in electrical engineering from the Pontifical Catholic University of Rio de Janeiro, Rio de Janeiro, Brazil, in 1989, and the Ph.D. degree in electrical engineering from the State University of Campinas, Campinas, Brazil, in 1994.

He is currently a Professor with the Institute of Technology, UFPA, and a Researcher with the Brazilian research funding agency National Council for Scientific and Technological Development (CNPq), Brasilia, Brazil. His research interests include electrical engineering, telecommunications, and computing.

Aldebaro Klautau (S'92–M'04–SM'08) received the Ph.D. degree from the University of California, San Diego, in 2003.

In 1995, he was a Faculty Member of the Federal University of Santa Catarina, Florianopolis, Brazil. Since 1996, he has been with the Federal University of Para, Belem, Brazil, where he is currently the Vice Director of the Department of Computer Engineering and affiliated with the Computer Science (PPGCC) and Electrical Engineering (PPGEE) Graduate Programs. He also directs the Signal Processing Laboratory (LaPS) and the Embedded Systems Laboratory (LASSE). His research interests include machine learning for signal processing, with applications to speech recognition, DSL, and software radio.

Dr. Klautau is a Cofounder and the current Chair of the IEEE Joint Chapter, North Brazil.

Klas Ericson received the Ph.D. degree in applied electronics from the Chalmers University of Technology, Gothenburg, Sweden, in 1984.

He has held various research and teaching positions in medical engineering and general measurements and modeling and administrative positions, e.g., as the Head of Operation, with some clinical engineering departments. He is currently with the Broadband Technologies Laboratory/Department, Ericsson A.B., Stockholm, Sweden. His research interests include measurement and modeling in an interdisciplinary setting, within which he has published some original refereed scientific papers and has filed some patents.

Jaume Rius i Riu received the M.Sc. degree in physics from the Autonomic University of Barcelona, Barcelona, Spain, in 1996, the M.S. degree in teaching and pedagogy from the University of Lleida, Lleida, Spain, in 1997, the Researcher Qualifying degree from the University of Barcelona, Barcelona, in 1998, and the Ph.D. degree in experimental physics from the Royal Institute of Technology, Stockholm, Sweden, in 2002.

In 2003, he was a Postdoctoral Fellow with the Department of Physics, Oulu University, Oulu, Finland. Since 2004, he has been with Ericsson A.B., Stockholm. From 2004 to 2006, he was the First Mile Technologies Work Package Leader with the European Union's 6FP MUSE Project, the Project Manager for a number of xDSL research projects, and a member of Ericsson's European Commission Research Steering Board and of support teams for broadband business case analysis and preparation. Since 2006, he has actively participated in Ericsson's broadband networks strategies and project planning. Since 2007, he has been Ericsson's Broadband Forum Standardization Coordinator and the Project Manager for Broadband Forum-Related Activities.

Dr. Riu is one of a member of the Industrial Research Group, Swedish Royal Academy of Engineering and Sciences (IFG IVA) and the Broadband Forum Broadband Convergence Oversight Committee.

Per Ola Börjesson received the Ph.D. degree in telecommunications theory from Lund University, Lund, Sweden, in 1980 and the Docent degree in telecommunications theory from Lund Institute of Technology, Lund, in 1983.

From 1988 to 1998, he was a Professor of signal processing with Luleå University of Technology, Luleå, Sweden. Since 1998, he has been a Professor of signal processing with the Department of Electrical and Information Technology, Lund University. He is currently researching on loop qualification and orthogonal frequency-division multiplexing (OFDM) or discrete multitone modulation with the Ericsson DSL Laboratory. His research work is focused on high-performance communication systems, in particular high-data-rate wireless and twisted-pair systems. He emphasizes the interaction between models and real systems—from the creation of application-oriented models based on system knowledge to the implementation and evaluation of algorithms. He has filed about ten patents and has published more than 50 original refereed scientific papers and conference proceedings, among which are highly cited works on synchronization and channel estimation for OFDM systems.